

Observation of superconductivity with T_c onset at 12K in electrically tunable twisted double bilayer graphene

Cheng Shen^{1,2}, Na Li^{1,2}, Shuopei Wang^{1,2,5}, Yanchong Zhao^{1,2}, Jian Tang^{1,2}, Jieying Liu^{1,2}, Jinpeng Tian^{1,2}, Yanbang Chu^{1,2}, Kenji Watanabe³, Takashi Taniguchi³, Rong Yang^{1,2}, Zi Yang Meng^{1,2,5}, Dongxia Shi^{1,2}, and Guangyu Zhang^{1,2,4,5*}

¹Beijing National Laboratory for Condensed Matter Physics and Institute of Physics, Chinese Academy of Sciences, Beijing 100190, China

²School of Physical Sciences, University of Chinese Academy of Sciences, Beijing 100190, China

³National Institute for Materials Science, 1-1 Namiki, Tsukuba 305-0044, Japan

⁴Beijing Key Laboratory for Nanomaterials and Nanodevices, Beijing 100190, China

⁵Songshan Lake Materials Laboratory, Dongguan, Guangdong 523808, China

*Corresponding author. Email: gyzhang@iphy.ac.cn

Electron-electron interactions play an important role in graphene and related systems to induce exotic quantum states, especially in a stacked bilayer with a small twist angle.¹⁻⁶ Under a magic twist angle in a bilayer graphene, flat band and strong many-body effects would lead to Mott-like insulating states and emergent superconductivity.⁴⁻⁶ Different from monolayer graphene, the band structure of AB-stacked bilayer graphene can be further tuned by displacement fields,^{7,8,9} providing an extra knob to realize the flat band in addition to the very sensitive twist angle. Here, we report the discovery and characterization of such displacement-field tunable twisted double bilayer graphene. Insulating states at half-filling for a wide range of twist angle and superconductivity with onset T_c at 12K, much higher than those observed in any other graphene heterostructures,

are observed. Furthermore, the resistance gap in the Mott insulator increases with respect to the in-plane magnetic fields and the as-measured g factor of ~ 2 suggests possible ferromagnetic fluctuations in the Mott phase which might mediate the corresponding unconventional pairing mechanism in the superconductivity phase observed in our system. These results establish the twisted double bilayer graphene as easily tunable platform for exploring new paradigm of quantum many-body states.¹⁰⁻¹⁷

Twisted bilayer graphene (TBG) with a small twist angle θ possesses significantly reconstructed band structure.^{1,2,3} In vicinity of a magic angle (MA), i.e. $\theta \approx 1.1^\circ$, strong interlayer hybridization leads to a flat band formation with low energy and narrow bandwidth, greatly enhances the electronic interaction effect^{1,4,5,6} than those of graphene or bilayer graphene without twisting.⁷ So far, correlated insulating states and superconductivity have been observed for a variety of partially filled bands,^{4,5,6} suggesting the TBG systems acquire novel features resembling strange metal in high- T_c superconductivity,^{5,10} novel states of the Mott insulator,^{4,11-15} unconventional and topological superconductor,^{5,16,17} (fragile) topological band structure,^{18,19} quantum anomalous Hall effect^{11,20} and many others, consequently spur the interests of theoretical and experimental communities alike. However, to observe these interesting correlation induced phenomena, one has to control θ accurately enough in TBG, which puts strict constraint in device fabrications. Therefore, easier access to the flat band by alternative approaches is of high importance. Recently, Mott insulator and superconductivity have been observed in TBG with $\theta > 1.1^\circ$ by exerting an external high pressure.⁶ Another approach is to apply vertical displacement electrical fields, achieved in ABC-stacked trilayer graphene on hexagonal boron nitride (hBN).^{21,22} However, tuning by displacement field fails in TBG, possibly due to strong interlayer hybridization.^{3,6}

Twisted double bilayer graphene (TDBG), on the other hand, is more likely to possess a flat band and display correlated phenomena.²³ It is known that monolayer graphene possesses linearly dispersive energy bands, showing no dependence on the displacement electrical fields. In contrast, AB stacked bilayer graphene shows parabolic band dispersion and gap opening at charge neutral point (CNP) could be induced under displacement electrical fields.^{7,8,9} The gap reaches its minimum not rightly at, but close to K point, displaying a “Mexican-hat” dispersion of band

structure.^{7,9} Such a dispersion hosts a narrower band width and could enable flat band formation in TDBG by displacement fields.

In this work, we report the success in easy tunability in TDBG by vertical electrical fields. At specific range of electric fields, we observe correlated Mott-like insulating state corresponding to the half-filled band on the electron branch, and more importantly, signatures of superconductivity with T_c onset at ~ 12 K and 50% resistance T_c at ~ 7 K in the vicinity of the Mott insulator. Our devices have the unique advantages that the characteristic temperature scales of Mott insulator and superconductivity are above the liquid helium temperature, therefore greatly reduced the requirement in device fabrications and sample characterizations. Moreover, under parallel magnetic fields, we found Mott gap for the half-filled band become stronger, suggesting a spin-polarized ordering and the correspondingly unconventional pairing mechanism of superconductivity.

TDBG samples were fabricated following a typical “tear and stack” technique²⁴ with θ accuracy at $\sim 0.1^\circ$. One-dimensional edge contact²⁵ was applied with a good characteristic less than $1 \text{ k}\Omega\cdot\mu\text{m}$. Figure 1a shows the schematic structure of our devices. Under proper displacement electrical fields, the reformed band structure of AB stacked bilayer graphene, hosts more flatness in the top of valence band and bottom of conduction band, and thus facilitate the formation of flat band in TDBG (Fig. 1b). All the devices are first picked out through their “U” shaped G–V_g curves at room temperature, which show greatly decreased carrier mobility because of the presence of flat band. .

We firstly tested two dual-gate devices with $\theta=1.28^\circ$ (device-1) and $\theta=1.31^\circ$ (device-2) to reveal the transport behavior of the half-filled insulating states in TDBG. Both devices show single-particle superlattice gap at $n=\pm n_s$ at electron and hole branch (Fig. 1c, 1d) (we note higher-order superlattice gaps at $n=\pm 3n_s$ are observed in device-3 with a smaller θ around 1.0°). The twist angle can be calculated through equation $A \approx \frac{\sqrt{3}a^2}{2\theta^2}$,^{4,5} where A is the area of moiré unit cell, extracted from magnetic flux where Landau levels cross or superlattice carrier density $n_s=4/A$, and $a=0.246\text{nm}$ is the lattice constant of graphene. The dual-gate structure makes it easier to tune carrier concentration as well as the displacement fields across TDBG. The displacement field is set by $D = \frac{1}{2}(D_t + D_b)$, where $D_t = +\epsilon_{rt}(V_t - V_t^0)/d_t$ and $D_b =$

$-\varepsilon_{rb}(V_b - V_b^0)/d_b$. Here, ε_{rt} and ε_{rb} are relative dielectric constant for top dielectric layer with thickness d_t , and bottom with d_b , respectively. V_t^0 and V_b^0 represent the offset gate voltage to reach the charge neutrality.

We can see an obvious insulating state at $n=n_s/2$ at electron branch under an intermediate D (Fig. 1c). Fitting through Arrhenius formula $R \sim e^{\frac{\Delta}{2kT}}$, the correlated gap in device-2 is estimated to be around 1meV, modified by displacement fields (Fig. 1d, inset) (We also note that the gap at half-filling varies with twist angle and device quality). Figure 1c also shows asymmetry for half-filled correlated states between electron and hole branches, hosted also by superlattice gap. From a band structure perspective, the electron-side flat band is well separated while hole-side flat band overlaps with other bands. This asymmetry presumably arises from an intrinsic asymmetry between valence and conduction bands in original bilayer graphene or a layer-polarized distribution of flat band.^{26,27} Besides, curves in Fig. 1c exhibit further asymmetry in resistance that slightly tuning of one gate would cause the curves cross each other at other partially filled superlattice point. This behavior suggests the presence of the lifted layer degeneracy or asymmetric layer-distribution of carriers.

The half-filled Mott-like insulating state can be further illustrated by Hall measurements. Under perpendicular magnetic fields, the sign of transverse magneto resistance signifies different carrier type. Figure 2a shows a switch of the carrier type at $n_s/2$, namely a zero Hall carrier concentration at $n=n_s/2$, suggesting that an emerging small Fermi surface originates from the half-filled insulating state and acquires an effective Hall carrier density. This small Fermi surface can also be identified by a new set of magneto oscillations which typically serves as a tool to obtain information about Fermi surface and degeneracy associated with electronic degrees of freedom, e.g. spin, valley and layer. Figure 2b explicitly shows one sided Landau levels (LLs) of filling factor $\nu=2, 4$ and 6, emanating from half-filled Mott states. The two-fold degeneracy of LLs, suggests only one preserved degeneracy while others are lifted for the upper Hubbard band, possibly due to ferromagnetic spin arrangement in the Mott insulator (will be discussed later). Moreover, a fully degeneracy-lifted LLs originated from CNP reveal enhanced e-e interactions,^{28,29,30} resulted from displacement fields D .

We proceed with providing a qualitative analysis about the electrical modulation mechanism. The exerted displacement fields would affect band structure by adding electrostatic potential difference between graphene layers and opening gap at charge neutrality for original AB stacked bilayer graphene.^{7,8,9} The electrostatic potential also closes the superlattice gap nearly linearly with D and even causes a “reentrant” behavior for hole-side superlattice gap (observed in our device-3). Figure 1c shows an enhanced insulating behavior at CNP, coherent with broken inversion-symmetry induced by electric fields. Synchronous emergence of Mott and charge neutral gap under almost identical displacement fields (Fig. 1c) confirms that the reformed band structure of the gapped ingredient bilayer graphene contributes to the formation of a separated flat band in TDBG, as mentioned above. While at high D , disappearance of flat band is possibly attributed to overlapping with other bands, overbended “Mexican hat” or trigonal warping effect,⁷ remained to be further uncovered.

The superconductivity in TDBG in device-1 with $\theta=1.28^\circ$ is discovered near the half-filled insulator. Figure 3a shows a representative R - T curve. At a low temperature $<4\text{K}$ the system develops zero resistance. The estimated T_c for 50% normal state resistance is about 7K, and T_c onset is about at 12K. Such high T_c in TDBG is above the liquid helium temperature and also much higher than the temperature scale of T_c in MA-TBG^{5,6} and ABC stacked trilayer graphene,²² this discovery certainly bestows one with confidence and points out direction to achieve even higher T_c in future experiments.

Figure 3b shows only one superconductivity pocket, located at electron side of half-filled insulator. The pocket shrinks with the increased temperature. Note that fluctuations around zero resistance possibly arises from inhomogeneous distribution of twist angle in our devices, which is also hosted in previous work.⁶ The inhomogeneity leads to the co-existence of insulator and superconductivity and finally forms stray capacitance which causes fluctuation of AC current phase during our measurements. Similar to the electrically tunable Mott insulator, superconductivity in TDBG can also be mediated by displacement fields, as depicted in Figure 3c. As we sweep the top gate voltage while keeping a constant back gate voltage varied from -16V to -31V, the zero resistance pocket shrinks and finally disappears. Thus a zero resistance behavior modulated by carrier density as well as displacement fields is present in TDBG.

Finally, we discuss the electronic nature of the half-filled Mott insulator and superconductivity in its vicinity. Since perpendicular fields affect not only spin but also orbital dynamics, to isolate the mechanism related with these correlated states, we instead exerted parallel magnetic fields in device-3 (graphite acts as back-gate) with $\theta=1.06^\circ$ and probe the field dependence in resistances. Fig. 4a shows absence of half-filled insulating state at $B_{//}=0\text{T}$ (Fig. 4a). The parallel magnetic fields monotonously enhance resistance at $n=n_s/2$ (Fig. 4c) and lead to an obvious insulating state at moderate D and higher $B_{//}$ (Fig. 4b, 4c). Since $B_{//}$ only affects spin degree of freedom, the enhanced insulating behavior implies the insulating state at $n_s/2$ is likely to be spin-polarized. Arising from Zeeman effect, magnetic fields induces gap $\Delta=g\mu_B B_{//}$, between spin-up and spin-down electrons, where the g factor for electrons in graphene is ~ 2 and μ_B is the Bohr magneton. From the Arrhenius formula of resistance, we obtain thermal activated gap as a function of $B_{//}$, which shows nearly linear increase as shown in Fig.4d. Thus we deduce the effective g factor is about 2.12, coincident with the expectation, and more importantly reveal the fact that the Mott gap is more likely to be spin-triplet gap, very different from the spin-singlet gap in the TBG system.^{4,6}

The above results support a spin-triplet Mott insulator state at $n=n_s/2$ in TDBG. Although in many cases Mott insulators are likely to be associated with the antiferromagnetic ordering. However, ferromagnetism can also be present in Mott insulators such as $\text{Ba}_2\text{NaOsO}_6$ ³¹ and $\text{Lu}_2\text{V}_2\text{O}_7$.³² Considering that the superconductivity occurs in the vicinity of the half-filled spin-polarized Mott-like state, a bold conjecture of ferromagnetic fluctuations mediated superconductivity in TDBG could be put forward. Such a case has been found in UGe_2 , where the superconductivity phase coexists with itinerant-electron ferromagnetic phase³³. Note that spin-triplet (valley-singlet in the case of TDBG) pairing superconductivity is also present in ^3He superfluid.^{34,35} Further investigations on TDBG, towards clarifying the ferromagnetism at $n_s/2$ and B -enhanced superconductivity, are now of utter most importance to verify the appealing conjecture presented here.

In summary, our work demonstrates electrically tunable half-filled Mott-like insulating state for a wide range of twist angle and superconductivity in TDBG, with estimated T_c for 50% normal state resistance at 7K and T_c onset at 12K. Our work suggests that TDBG hence provides an alternative, maybe easier, approach to observe

correlated insulators and superconductivity in graphene heterostructures. The hypothesized spin-polarized ground state, different from that in MA-TBG, reveals an important role played by layer numbers of the original constituent 2D materials in twist system. Such interesting presence of possibly spin-polarized correlated insulating state and superconductivity with much higher T_c are calling for further theoretical and experimental efforts to reveal the underlying mechanism and the avenue of further investigating correlated quantum many-body states in TDBG is now lying ahead of the community.

Reference

- 1 Bistritzer, R. & MacDonald, A. H. Moiré bands in twisted double layer graphene. *Proc. Natl. Acad. Sci.* **108**, 12233-12237(2011).
- 2 Cao, Y. et al. Superlattice-induced insulating states and valley protected in twisted bilayer graphene. *Phys. Rev. Lett.* **117**, 116804(2016).
- 3 Kim, K. et al. Tunable moiré bands and strong correlations in small twist angle bilayer graphene. *Proc. Natl. Acad. Sci.* **114**, 3364-3369(2017).
- 4 Cao, Y. et al. Correlated insulator behaviour at half-filling in magic-angle graphene superlattices. *Nature* **556**, 80-84(2018).
- 5 Cao, Y. et al. Unconventional superconductivity in magic-angle graphene superlattices. *Nature* **556**, 43-50(2018).
- 6 Yankowitz, M. et al. Tuning superconductivity in twisted bilayer graphene. *Science* **363**, 1059-1064(2019).
- 7 Castro Neto, A. H., Guinea, F., Peres, N. M. R., Novoselov, K. S. & Geim, A. K., The electronic properties of graphene. *Rev. Mod. Phys.* **81**, 109-162(2009).
- 8 Zhang, Y. et al. Direct observation of a widely tunable bandgap in bilayer graphene. *Nature*, **459**, 820–823(2009).
- 9 Castro, E. V. et al. Biased bilayer graphene: semiconductor with a gap tunable by the electric fields effect. *Rev. Phys. Lett.* **99**, 216802(2007).
- 10 Cao, Y. et al. Strange metal in magic-angle graphene with near Planckian dissipation. arXiv:1901.03710.
- 11 Sharpe, A. L., et al. Emergent ferromagnetism near three-quarters fillings in twisted bilayer graphene. arXiv:1901.03520.
- 12 Xu, X. Y., Law, K. T. & Lee, P. A. Kekulé valence bond order in an extended

- Hubbard model on the honeycomb lattice with possible applications to twisted bilayer graphene, *Phys. Rev. B* **98**, 121406(R) (2018).
- 13 Liao, Y. D., Meng, Z. Y. & Xu, X. Y. Is magic-angle twisted bilayer graphene near a quantum critical point? arXiv:1901.11424.
 - 14 Koshino, M., Yuan, N. F. Q., Koretsune, T., Ochi, M., Kuroki, K. & Fu, L. Maximally localized Wannier orbitals and the extended Hubbard model for twisted bilayer graphene, *Phys. Rev. X* **8**, 031087 (2018).
 - 15 Po, H. C., Zou, L., Vishwanath, A. & Senthil, T. Origin of Mott insulating behavior and superconductivity in twisted bilayer graphene, *Phys. Rev. X* **8**, 031089 (2018).
 - 16 Xu, C. & Balents, L. Topological superconductivity in twisted multilayer graphene. *Phys. Rev. Lett.* **121**, 087001(2018).
 - 17 Liu, C-C., Zhang, L-D., Chen, W-Q. & Yang, F. Chiral spin density wave and $d + id$ superconductivity in the magic-angle-twisted bilayer graphene. *Phys. Rev. Lett.* **121**, 217001(2018).
 - 18 Po, H. C., Zou, L., Senthil, T., & Vishwanath, A. Faithful tight-binding models and fragile Topology of magic-angle bilayer graphene, arXiv:1808.02482.
 - 19 Zhang, Y.-H., Mao, D., Cao, Y., Jarillo-Herrero, P. & Senthil, T. Nearly flat Chern bands. *Phys. Rev. B* **99**, 075127 (2019).
 - 20 Zhang, Y-H., Mao, D. & Senthil, T. Twisted bilayer graphene aligned with hexagonal boron nitride: anomalous Hall effect and a lattice model, arXiv:1901.08209.
 - 21 Chen, G. et al. Evidence of a gate-tunable Mott insulator in trilayer graphene moiré superlattice. *Nat. Phys.* **15**, 237–241(2019).
 - 22 Chen, G. et al. Signatures of gate-tunable superconductivity in trilayer graphene/boron nitride moiré superlattice. arXiv:1901.04621.
 - 23 Chebrolu, N. R., Chitarri, B. L. & Jung, J. Flatbands in twisted bi-bilayer graphene. arXiv:1901.08420.
 - 24 Kim, K. et al. van der Waals Heterostructures with high accuracy rotational alignment. *Nano. Lett.* **16**, 1989-1995(2016).
 - 25 Wang, L. et al. One-dimensional electrical contact to a two dimensional material. *Science* **342**, 614-617(2013).
 - 26 Li, Z. Q., Henriksen, E. A., Jiang, Z., Hao, Z., Martin, M. C., Kim, P., Stormer, H. L. & Basov, D. N. Band structure asymmetry of bilayer graphene revealed by infrared spectroscopy. *Phys. Rev. Lett.* **102**, 037403(2009).

- 27 Choi, Y. W. & Choi, H. J. Intrinsic band gap and electrically tunable flat bands in twisted double bilayer graphene. arXiv:1903.00852.
- 28 Zhao, Y., Cadden-Zimansky, P., Jiang, Z. & Kim, P. Symmetry breaking in the zero-energy Landau level in bilayer graphene. *Phys. Rev. Lett.* **104**, 066801(2010).
- 29 Feldman, B. E., Martin, J. & Yacoby, A. Broken-symmetry states and divergent resistance in suspended bilayer graphene. *Nat. Phys.* **5**, 889-893(2009).
- 30 Young, A. F. et al. Spin and valley quantum Hall ferromagnetism in graphene. *Nat. Phys.* **8**, 550-556(2012).
- 31 Erickson, A. S. et al. Ferromagnetism in the Mott insulator $\text{Ba}_2\text{NaOsO}_6$. *Phys. Rev. Lett.* **99**, 016404(2007).
- 32 Shamoto, S., Nakano, T., Nozue, Y. & Kajitani, T. Substitution effects on ferromagnetic Mott insulator $\text{Lu}_2\text{V}_2\text{O}_7$. *J. Phys. Chem. Solids.* **63**, 1047-1050(2002).
- 33 Saxena, S. S. et al. Superconductivity on the border of itinerant-electron ferromagnetism in UGe_2 . *Nature*, **406**, 587-592(2000).
- 34 Leggett, A. J. A theoretical description of the new phases of superfluid ^3He . *Rev. Mod. Phys.* **47**, 331(1975).
- 35 Wheatley, J. C. Experimental properties of superfluid ^3He . *Rev. Mod. Phys.* **47**, 415(1975).

Methods

Sample preparations. Raw materials of bilayer graphene, hexagonal boron nitride (20-35nm in thickness) and graphite flakes were first exfoliated on SiO_2 (300nm thick), then annealed in Ar/H_2 mixture at temperature up to 450°C for cleanness. Usually, moderate H_2 plasma etching was also applied to fully get rid of contaminations coming from the exfoliation process. We used Poly (Bisphenol A carbonate) (PC) supported by Polydimethylsiloxane (PDMS) on glass slide to pick up boron nitride firstly and then tear and pick up bilayer graphene. The home-made micro-position stage can control the rotation angle at 0.1° error range. We performed no annealing for TDBG as it tends to relax to nearly twist angle $\theta=0^\circ$ once temperature is high. The fabrication of metal top gate and electrodes follows a standard e-beam lithography and e-beam metal evaporation. Devices were designed as Hall bar structure and shaped by traditional reactive ion etching with CHF_3 and O_2

mixture gas. Here, the metal top gate also acts as a mask for etching to ensure the channel is fully gated. Finally, all the bars were contacted through one-dimensional edge contact with Cr/Au electrodes.

Measurements. Transport measurements were performed in cryostat with a base temperature of 1.5K. We applied standard lock-in techniques with 31Hz excitation frequency and less than 200uV AC excitation bias voltage which is achieved by a 1/1000 voltage divider. All the transport data were acquired by four-terminal measurements.

Author contributions

G.Z. supervised this work. C.S. conceived of this project, fabricated the devices, performed the transport measurements and data analysis. K.W. and T.T. provided hexagonal boron nitride crystals. C.S., Z.Y.M. and G.Z. wrote the paper. All the other authors are involved in the discussion on this work.

Acknowledgements

We appreciate the helpful discussion with Guorui Chen in UC Berkeley and Shiliang Li at Institute of Physics, Chinese Academy of Sciences. G.Z. thanks the financial supports from NSFC under the grant No. 11834017 and 61888102, the Strategic Priority Research Program of CAS under the grant No. XDB30000000, the Key Research Program of Frontier Sciences of CAS under the grant No. QYZDB-SSW-SLH004, and the National Key R&D program under grant No. 2016YFA0300904. Z.Y.M. acknowledges supports from the National Key R&D Program (2016YFA0300502), the Strategic Priority Research Program of CAS (XDB28000000) and the NSFC (11574359). K.W. and T.T. acknowledge support from the Elemental Strategy Initiative conducted by the MEXT, Japan, A3 Foresight by JSPS and the CREST (JPMJCR15F3), JST.

Figures and Figure captions

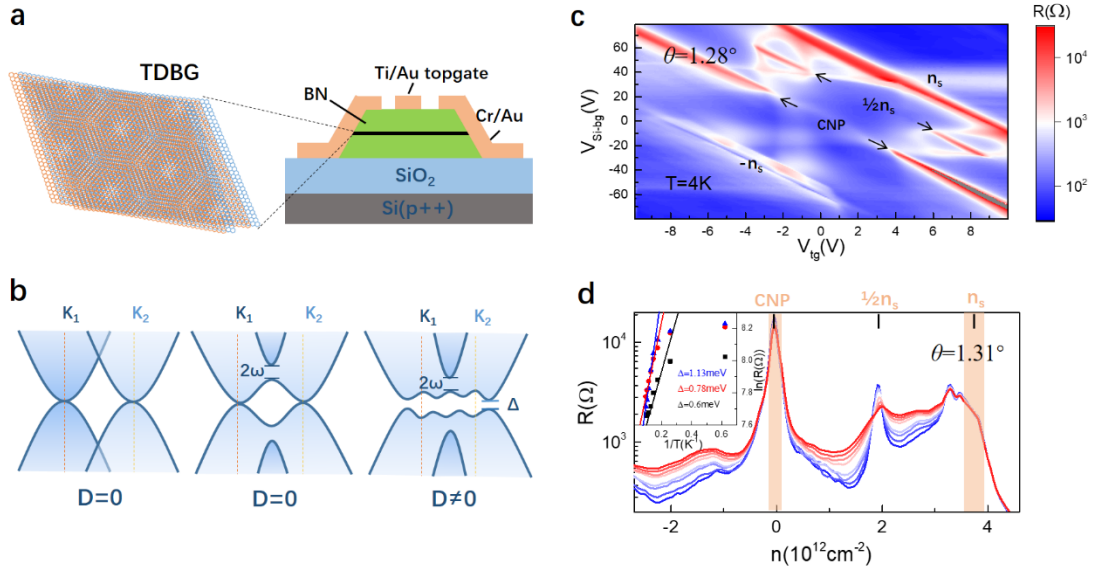


Figure 1| Half-filled insulating state tuned by displacement fields. (a), Schematic device structure. (b), Pedagogical illustration of electrical tuning mechanism. $2w$ and Δ are hybridization energy and gate-tunable band gap in AB stacked bilayer graphene, respectively. (c), Color plot of resistance versus metal top-gate and Si back-gate voltages in device 1 with $\theta=1.28^\circ$ at $T=4\text{K}$. (d), Temperature-dependent R - V_{tg} curves for device 2 with $\theta=1.31^\circ$ with T varying from 1.61K (dark blue curve) to 11K (dark red curve). V_{bg} is fixed at 55V while the top-gate voltage is swept for all the curves. The enhancement of resistance as temperature cools down, reflects the insulating behavior at $n_s/2$. Inset shows thermal activated gap at $n_s/2$ fitted through Arrhenius formula $R \sim \exp[\Delta/(2kT)]$. The fitted gap is 0.6meV, 0.78meV, 1.13meV for displacement fields $D=0.297\text{V/nm}$ (black), 0.353V/nm (red) and 0.409V/nm (blue), respectively.

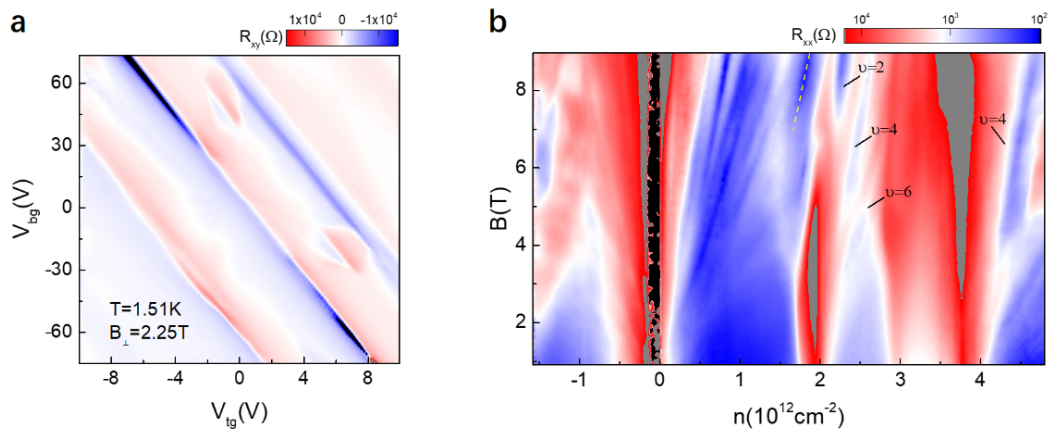


Figure 2| Quantum oscillations in TDBG. (a), Transverse Hall resistance as a

function of top and back gate voltages for device 2 with perpendicular fields $B=2.25\text{T}$ applied. Hall resistance changes sign at $n_s/2$, featuring zero Hall carrier density. **(b)**, Quantum oscillations of longitudinal resistance under perpendicular magnetic fields up to 9T for device 1. V_{tg} is fixed at 8V and the back-gate voltage is swept to modulate carrier concentration. Three sets of Landau fan emanate from CNP, $n_s/2$ and n_s . Landau fan features a totally lifted degeneracy near CNP and LLs of $\nu=2,4,6,\dots$ near $n_s/2$. While for superlattice point, we can just ensure a dominant LL of $\nu=4$. LL is marked by orange dash line presumably indicates the Hofstadter butterfly effect. A potential presence of $3n_s/4$ insulating state is pointed towards by maximum of magneto resistance at $3n_s/4$.

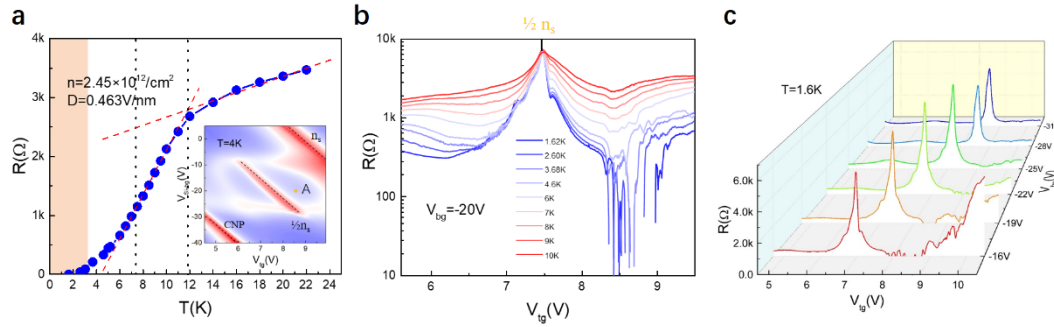


Figure 3| Zero resistance behavior near $n_s/2$. **(a)**, R-T curve for device 1 at fixed carrier density and displacement fields illustrated as orange dot A in the inset picture. The onset temperature of superconductivity is at 12K, the 50% resistance temperature of superconductivity is at 7 K, denoted by the black dashed lines. **(b)**, Temperature-dependent transport behavior at carrier density near $n_s/2$. The back Si gate is fixed at -20V. The resistance at n-side of half-filled insulating state fluctuates around zero when temperature is below about 4K. **(c)**, Transport behavior at carrier density near $n_s/2$ as a function of back gate and top gate. When the top gate is set up to 25V, zero resistance, i.e., superconductivity disappears.

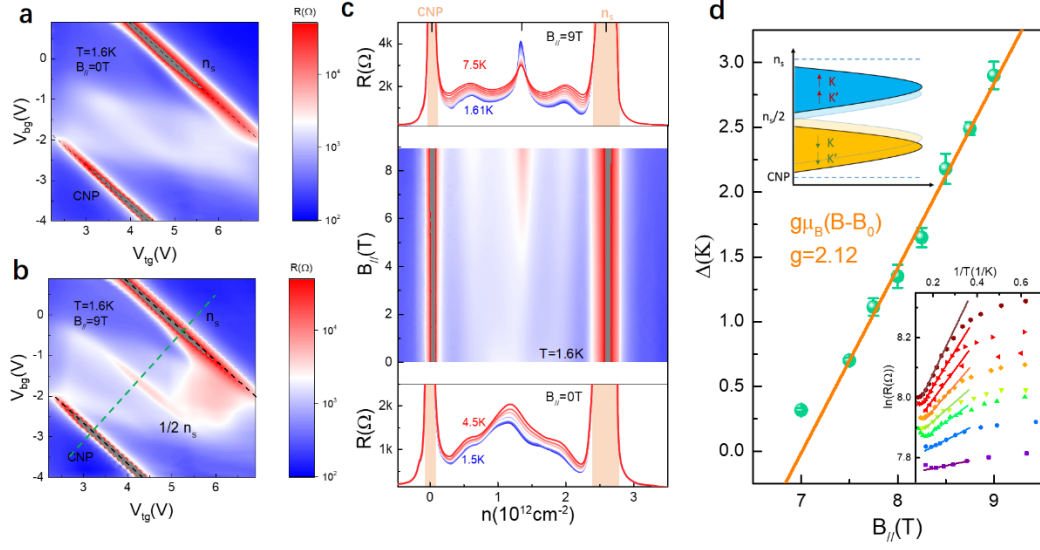


Figure 4| Parallel magnetic fields dependence of $n_s/2$ correlated insulating state.

(a), (b), Resistance color plot as a function of top and bottom metal gate voltage for device 3 (measured between Hall bars with $\theta=1.06^\circ$) under parallel magnetic fields $B_{||}=0T$ (a) and $B_{||}=9T$ (b). (a) and (b) share the same color scale bar. The dark dot lines in (a) and (b) represent resistance maximum at CNP and n_s , respectively. When $B_{||}=9T$ is applied, resistance maximum at $n_s/2$ appears. Top and back gate voltage sweeping along the green dot line in (b), linearly changes carrier density while keeping the displacement fields D constant as $D=0.306V/nm$. (c), Resistance for $D=0.306V/nm$ enhanced by parallel magnetic fields. The top and bottom figures in (c) show temperature-dependent behavior at $B_{||}=9T$ and $B_{||}=0T$, respectively. (d), When $B_{||}$ is large enough, gap of $n_s/2$ insulating state can be thermal fitted (shown the bottom inset figure) and nearly follows a linear variation with $B_{||}$. Such field dependence suggests a possible spin-polarized Mott insulator state. The top inset elucidates such state at $n_s/2$. Single-particle flat band is split into upper and lower spin-degeneracy lifted Hubbard bands by e-e interactions. Zeeman effect broadens the correlated gap between Hubbard bands by $g\mu_B B$.